I. Ahmed<sup>1</sup>, H. Poudyal<sup>1</sup>, A. J. Chandy<sup>2</sup>\*

# Fill Factor Effects in Highly-Viscous Non-Isothermal Rubber Mixing Simulations

A finite volume technique in a commercial computational fluid dynamics (CFD) code is employed in this study to simulate transient, incompressible, non-Newtonian and non-isothermal rubber mixing. The simulation processes are conducted in a two-dimensional(2D) domain, where a mixing chamber partially-filled with rubber is equipped with a pair of two-wing non-intermeshing counter-rotating rotors. The main objective is to assess the effect of different fill factors of rubber on dispersive and distributive mixing characteristics by simulating 15 revolutions of the rotors rotating at 20 min<sup>-1</sup>. 50%, 60%, 70%, 75%, 80% and 90% are the six different fill factors chosen for the study. An Eulerian multiphase method has been applied to solve for the two different phases, rubber and air. The non-Newtonian property of rubber is handled using the shear rate dependent Carreau-Yasuda model, along with an Arrhenius function to include the temperature dependency. In addition to the governing equations related to the conservation of mass, momentum and energy, the volume of fluid (VOF) method is chosen to track the interface between air and rubber. With regard to the results, flow patterns, thermal distributions, viscosity behavior and volume fraction are analyzed for the different fill factors. In addition, dispersive and distributive mixing behavior is also assessed in detail using Lagrangian statistics, such as mixing index, cumulative distribution of maximum shear stress, cluster distribution index (CDI), scale of segregation (SOS) and length of stretch (LOS), calculated from massless particles. Both the Eulerian and Lagrangian results showed that fill factors between 70% and 80% presented the most reasonable and efficient mixing scenario, and also exhibited the best dispersive and distributive mixing characteristics combined.

#### 1 Introduction

Mixing of highly viscous materials such as rubber and other kinds of elastomers is a critical and basic step in the entire manufacturing process involving such materials. By definition, mixing is a process that will enhance some basic engineering

properties such as mechanical, chemical, and physical properties by reducing the non-uniformity of the ingredients, which in turn will affect the throughput as well as the final product quality (Tadmor and Gogos, 2013). For rubber industries like tire manufacturing, mixing is represented by compounding rubber, which is mainly synthesized from petroleum by products (Alsteens et al., 2003), with different types of solid and liquid additives. The high viscosity of rubber results in significant internal heat dissipation. Hence, an isothermal assumption might not be appropriate for such problems (Malkin et al., 1999). There are typically different types of mixing devices used for high viscosity mixing (see US patents, US1689990 A, US1260684 A, US2067458 A, US2015618 A, US5158725 A, US2694224 A). Various factors that affect the performance of mixing include the size and shape of the mixing chamber, rotor speed, speed ratio (with two rotors rotating with different speeds), fill factor (volume percentage of rubber inside the chamber), and ram pressure all affect the flow field and in turn the mixing efficiency (Das et al., 2016), and the two primary mixing mechanisms include dispersive and distributive mixing mechanisms (Manas-Zloczower et al., 1984).

Dispersiveness of mixing in a system indicates the manner in which particles are dispersed in a continuous phase. On the other hand, distributive mechanism refers to the spreading of all the ingredients throughout the domain (Wang and Manas-Zloczower, 2001). The rotating motion of rotors increases shear, which breaks down the agglomerate constituting the rubber and other filler materials. This is called dispersion, which is mainly achieved by shear and elongational forces. Several studies have shown that elongational flow is more effective in comparison with simple shear flow, for dispersion (Manas-Zloczower, 1997). Quantities such as mixing index and maximum shear stress can help quantify the dispersive characteristics, and are presented in this study. For investigating distributive mixing though, a large set of massless particles are introduced into the mixing chamber for a period of time to calculate statistics such as cluster distribution index (CDI) and scale of segregation (SOS). For analyzing the efficiency of mixing, length of stretch (LOS) is also presented and finally, for assessing the viscous heat dissipation, the thermal distribution is analyzed as well.

There have been previous experimental studies that have focused on quantifying the dispersive and distributive mechanisms of mixing (Collin et al., 2006; Cotten, 1984; Kim and White, 1989; Leblanc and Lionnet, 1992; Limper and Hesse,

<sup>&</sup>lt;sup>1</sup>Department of Mechanical Engineering, University of Akron, Akron, Ohio, USA

<sup>&</sup>lt;sup>2</sup> Department of Mechanical Engineering, Indian Institute of Technology Bombay, Mumbai, Maharashtra, India

<sup>\*</sup> Mail address: Abhilash J. Chandy, Department of Mechanical Engineering, Indian Institute of Technology Bombay, Mumbai, Maharashtra, 400076, India E-mail: achandy@iitb.ac.in

2005; Nikiel et al., 2016). For instance, Limper and Hesse (2005) experimentally assessed the effect of rotor design on dispersive and distributive mixing. Collin et al. (2006) experimented with different initial sized pellets to assess its effect on dispersive mixing, and results were also compared with numerical simulations. With the advent of very powerful computers over the past decade, numerical simulations of such problems are becoming more feasible, and are more cost-effective and convenient to setup compared to experiments.

A lot of numerical studies have also been conducted in the past (Alsteens et al., 2003; Avalosse and Rubin, 2000; Cheng and Manas-Zloczower, 1998; 1990; 1989; Connelly and Kokini, 2004; 2007; Dhanasekharan and Kokini, 2003; Emin and Schuchmann, 2012; Rathod and Kokini, 2013; Salahudeen et al., 2011; Takeshi et al., 2002; Vyakaranam and Kokini, 2012; Yang and Manas-Zloczower, 1994). Among those, Cheng and Manas-Zloczower (1989) studied the velocity and pressure profile of a 2D Banbury mixer using a finite element method. They also developed a model to assess the effect of rotational speed, gap size and speed ratio on the flow characteristics and distributive mixing as well (Cheng and Manas-Zloczower, 1998; 1990). The effect of changing gap on distributive and dispersive mixing efficiency was assessed by Yang and Manas-Zloczower (1994) by using a variable intermeshing clearance. Connelly and Kokini (2004) studied dough mixing using finite element methods and analyzed the ability of single and twin screw extruders. They also examined the effects of rheology with different viscoelastic and shear thinning models and assessed the effectiveness of mixing through statistical tools such as segregation scale, cluster distribution index, mixing index, length of stretch and efficiency of mixing (Connelly and Kokini, 2007). A detailed comparative study of three different rotor designs: cam, banbury and roller was carried out by analysing velocity profiles and particle trajectories by Salahudeen et al. (2011). All these studies assumed a fully-filled mixing chamber, which practically is never the case.

There have been however a few studies more recently, involving a partially filled mixing chamber. One study on partially-filled mixing was by Fukutani (2013), where they measured flow rates to assess distributive mixing for two different fill-factors, while employing the volume of fluid (VOF) method for the calculation of the free surface. Liu et al. (2015) in their VOF calculations investigated partially-filled flow of a rubber compound and observed voids behind the rotor wings, and material exchange occurring in the middle of the chamber. In addition, the current research group has also been involved in several partially-filled mixing calculations of rubber compounds (Das et al., 2016; Das et al., 2017; Dhakal et al., 2017). All these studies assumed isothermal mixing.

There have been a few numerical studies performed under non-isothermal conditions as well. Non-Newtonian and non-isothermal flow simulation codes were developed in twin screw extruders using the finite element method, which could simulate the fully-filled part of several kinds of screw elements, such as full flight screws, kneading discs, rotors, and their combinations (Takeshi et al., 2000; 2001). Nassehi and Ghoreishy (2001) studied the non-isothermal mixing of a non-Newtonian fluid in a partially-filled 2D intermeshing type mixing device, by calculating the free surface using a finite element method coupled with an Eulerian-Lagrangian method.

3-D transient fully-filled numerical simulations of twin screw extruder configurations were presented in Avalosse et al. (2002), including an analysis of different non-isothermal features that characterize the flow induced by a co-rotating as well as a counter-rotating configuration. Bai et al. (2011) studied the temperature distribution and heat transfer mechanism for a fully-filled mixing chamber under non-isothermal conditions. Also, the effect of rotor speed on distributive and dispersive mixing in a partially-filled non-isothermal mixing chamber was studied by Poudyal et al. (2016). There are several advantages to modeling partially-filled rubber mixing with applications to manufacturing, using a non-isothermal model. Firstly, it represents a more realistic scenario from a manufacturing standpoint. Secondly, this representation can provide information about mixing time limits with impact on the overheating of material and device.

So the main goal of this study is to develop a two dimensional (2D) computational fluid dynamics (CFD) model to assess the effect of different fill factors on distributive and dispersive mixing characteristics of rubber mixing chamber in non-isothermal conditions. While a 2D model is not entirely representative of the practical mixing scenario due to the absence of the axial direction for any material movement, such calculations can still provide a lot of valuable insights into the effects of various operating conditions on mixing efficiency, at a relatively lower cost. For instance, the computational time of a 3D calculation with the equivalent grid and particle distribution would be at least five times that of a typical 2D calculation presented here. Fill factor, which is the volumetric percentage of rubber in the mixing chamber, is a very important parameter for mixing efficiency. For under-filled conditions, the ram of the mixing device is not able to create enough pressure for achieving shear mixing, and over-filled conditions restrict the ram to reach the bottom of the chamber. This makes fill factor a critical parameter for optimizing mixing (Dhakal, 2016). To the authors' knowledge, there have not been any studies performed yet dealing with fill factors under non-isothermal conditions. For varying the fill-factors, the volume percentage of rubber with respect to the entire mixing chamber is varied and the rest of the chamber is filled with air. The fill factors investigated in this study are 50%, 60%, 70%, 75%, 80% and 90%. The other assumptions include considering rubber as a homogeneous non-Newtonian Carreau-Yasuda fluid for simplicity.

## 2 Geometry and Materials

The geometry consists of a mixing chamber equipped with a set of two-wing non-intermeshing rotors. Figure 1A shows the complete schematic in 3D of the rotors, which are oriented at 180° with respect to each other. For this study, a 2D cross-section created at the middle of the vertical axis of the rotor, as shown in Fig. 1A, is employed. The cross-section itself is shown in Fig. 1B. Note that a 2D cross-section at the centre is chosen arbitrarily in this study. If it were chosen at a different location, the geometry would differ and consequently, the results would be different. However, the conclusions with respect to the fill factor performance would possibly stay the same for a specific geometry. To prove this though, one has to carry out an additional set of fill factor calculations with a different

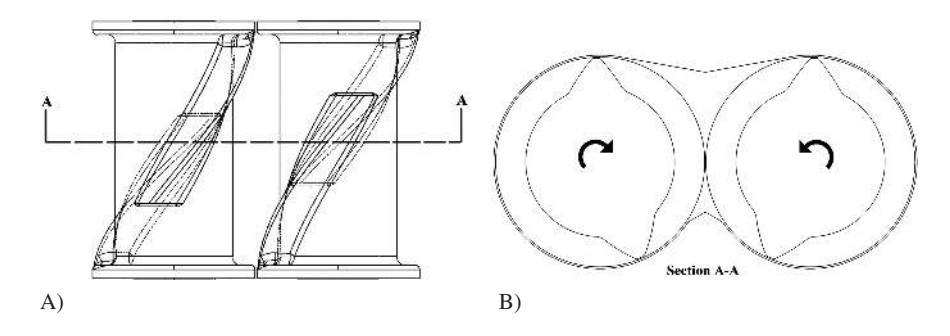


Fig. 1. Two-wing counter-rotating rotor geometry showing the (A) 3D model, and (B) 2D mid-cross section across A-A employed in the current study

2D cross-section (or geometry), which is beyond the scope of this study. Here, the left and right rotors counter-rotate about their own axes. Each rotor has a radial dimension of 278 mm with a clearance of 8 mm in between rotor tip and the chamber wall. This is a typical rotor used for batch mixing processes in the polymer industry. The basic design of this rotor is based on the U.S. Patent 4,714,350, and the design parameters can be found in the patent (Wu, 1971).

The material properties are chosen from a previous study of the same research group (Das et al., 2016). The main ingredient here is rubber. The chamber is assumed to be partially filled with incompressible, non-Newtonian rubber at different fill factors representing the different cases investigated here. The density of rubber is chosen to be  $\rho_1=1\,100\,kg/m^3$ . The viscosity of rubber is estimated with the Carreau Yasuda model (Vingaard et al., 2007) (see the next section for details). Besides rubber, the rest of the chamber is assumed to be filled with air, which is assumed to be an ideal gas. The density of air is chosen as  $\rho_2=1.18\,kg/m^3$ , with a constant dynamic viscosity of  $\mu_2=1.86\times10^{-5}$  Pa s. The axis of rotation is assumed to be horizontal, which is the reason why rubber is filled at the bottom end of section A-A due to gravity.

The non-Newtonian as well as physical and thermal properties of the rubber are shown in Tables 1 and 2, respectively.

#### **3 Governing Equations**

For the numerical solution presented here, the governing equations of mass, momentum and energy are solved. The conservation of mass or the continuity equation is given by Eq. 1, conservation of momentum is given by Eq. 2, and due to the non-isothermal conditions, the conservation of energy is solved and is given by Eq. 3.

$$\frac{\partial \rho}{\partial t} + \nabla \cdot (\rho \mathbf{V}) = 0, \tag{1}$$

Density	Thermal conductivity	Specific heat	
kg/m <sup>3</sup>	W/m K	J/kg K	
1 100	0.25	1400	

Table 2. Physical and thermal properties of rubber

$$\frac{\partial(\rho \mathbf{V})}{\partial t} + \nabla \cdot (\rho \mathbf{V} \mathbf{V}) = -\nabla p + \nabla \cdot \boldsymbol{\tau} + \rho \mathbf{g}, \tag{2}$$

$$\partial(\rho C_p T)\partial t + \nabla \cdot (\mathbf{V} \rho C_p T) = \nabla \cdot (k \nabla T) + \mathbf{\tau} : \nabla \mathbf{V}, \tag{3}$$

Here  $\rho$  is the density, t is time, **V** is velocity vector,  $\sigma$  is Cauchy's stress tensor, g is acceleration due to gravity,  $C_p$  is specific heat, T is temperature, and k is thermal conductivity. The tensor product,  $\tau : \nabla V$ , is the viscous dissipation and  $\tau$  is the viscous stress tensor, given by:

$$\tau = 2\mu \mathbf{D}.\tag{4}$$

Here D is strain tensor, defined as:

$$\mathbf{D} = \frac{1}{2} \left[ \nabla \mathbf{V} + \nabla \mathbf{V}^{\mathrm{T}} \right]. \tag{5}$$

The viscosity of non-Newtonian rubber considered here,  $\mu$ , is shear dependent and can be estimated using the non-Newtonian Carreau-Yasuda model (Vingaard et al., 2007), which is defined as:

$$\mu = \mu(\dot{\gamma}) = \mu_{\infty} + (\mu_0 - \mu_{\infty})(1 + (\lambda \dot{\gamma})^2)^{(n-1)/2}. \eqno(6)$$

Here, the power constant, n = 0.4, the zero-shear viscosity,  $\mu_0 = 100,000$  Pa s, the infinite-shear viscosity,  $\mu_\infty = 100$  Pa s, and the relaxation time constant,  $\lambda = 10$  s (Goodyear, 2015; Das et al., 2016; 2017; Dhakal et al., 2017). Here,  $\dot{\gamma}$  is the shear rate, defined as:

$$\dot{\gamma} = \sqrt{(2\mathbf{D} : \mathbf{D})}.\tag{7}$$

Time constant s	Power-law index	Zero shear viscosity kg/m s	Infinite shear viscosity kg/m s	Reference temperature K	Activation energy K
10	0.4	100,000	100	373	876

Table 1. Non-Newtonian rubber properties

Also, note that while rubber compounds are indeed viscoelastic in nature (Manas-Zloczower, 2012; Osswald and Hernández-Ortiz, 2006), their viscoelastic response is not taken into account here in order to reduce the computational complexity in terms of a tractable solution. Future investigations of partially-filled rubber mixing could include the effect of viscoelasticity into the model.

Due to the non-isothermal conditions, the zero-shear viscosity,  $\mu_0$ , in Eq. 6 is temperature-dependent, and is defined by using an Arrhenius function as follows:

$$\mu_0(T) = Ae^{\left(\frac{E_a}{RT}\right)},\tag{8}$$

where the material constant, A = 99,185, activation energy,  $E_a = 876$  K, and R is molar gas constant = 287 J/kg K.

Since the chamber modeled here is partially-filled with non-Newtonian rubber with the rest of the chamber filled with air, it is necessary to track the rubber-air interface. This interface is solved by using the Eulerian-based VOF method. The two different phases (rubber and air) are governed by a single continuity and momentum equation, but the volume fraction (fraction of the volume of fluid in a cell as a function of the total volume of cell) of each phase is tracked within each individual cell throughout the domain. In the absence of any source/sink terms for the volume fraction evolution, the formulation of VOF is given by:

$$\frac{\partial C_m}{\partial t} + V \cdot \nabla C_m = 0, \tag{9}$$

where  $C_m$  is the volume fraction of  $m^{th}$  phase. Also, mixing quantities such as length of stretch, cluster distribution index, cumulative distribution of maximum shear stress are calculated by injecting a set of massless particles. For tracking the positions of these particles, an interpolation scheme from the velocity field has been applied, which is defined as:

$$\frac{dx}{dt} = u_p, \tag{10}$$

where  $u_p$  is the particle velocity.

### 4 Computational Model

A commercial CFD software is used to simulate rubber compound mixing in a chamber equipped with non-intermeshing, two-wing rotors, under non-isothermal conditions. The two wings are counter-rotating at a constant speed of 20 rpm and the left rotor rotates in the clockwise direction. The mixing chamber is partially-filled with Carreau-Yasuda described rubber, with the rest of the volume occupied by air. A total of six simulations are carried out with different fill factors of rubber and are presented here. The fill factors are 50%, 60%, 70%, 75%, 80% and 90%. Figure 2 shows how the rubber is initially filled for the different fill factor cases. Note that the y direction is considered to be the direction of gravity.

With regard to the mesh, a combination of structured quadrilateral and triangular mesh elements that constitute 200,274 in number is used. To ensure adequate mesh resolution and resolve the high velocity gradients, an additionally finer mesh is created between the rotor tip and chamber wall. This region does play an important role in the heat generation in such problems, which can indeed be analyzed with the non-isothermal model here. Figure 3 shows the mesh for the entire domain. In addition, the mesh in the region between rotortip and boundary wall is also shown in order to indicate the finer mesh resolution in this critical area. The grid resolution employed for these simulations was chosen after conducting a mesh-independence study using three different resolutions as was done in the authors' past studies as well (Das et al., 2016; Dhakal et al., 2017). In addition, the CFD model developed here for partially-filled rubber mixing has been validated qualitatively and quantitatively with previous experiments (see the authors' previous studies for a specific description of these validation studies (Das et al., 2017; Dhakal et al., 2017)).

In order to achieve rotational motion of the rotors, a moving mesh technique is used. In this technique, the fluid region encompassing the rotors rotates, while the rest of the fluid region stays unmoved. Hence, a direct interface between these fluid

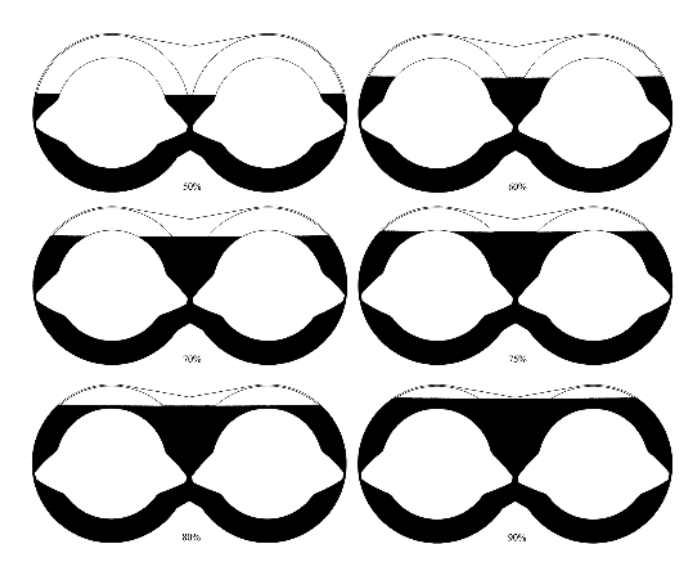


Fig. 2. Initial representation of the different fill factor calculations presented in this study

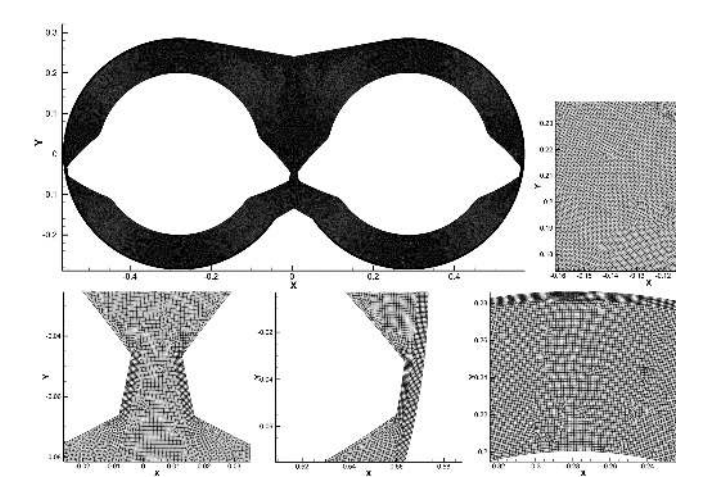


Fig. 3. Structured quadrilateral and triangular mesh for the different parts of the computational domain

regions is created such that mass can transfer through the interface. The two zones, which are the ones made up of the rotor and the region between the rotor and the chamber itself, will move relative to each other along the mesh interface. As the rotor rotates, the implementation does not require node alignment along the mesh interface. The Reynolds number, Re is very small ( $\ll 1$ ), owing to the fact that rubber has an extremely high viscosity, implying laminar flow. The momentum and energy equations are spatially discretised using second order unwinding and temporally discretised using an implicit first order method. For solving pressure and velocity, a segregated solver is used and the PISO scheme is employed for the pressure-velocity coupling. An Eulerian multiphase model based on the volume of fluid (VOF) technique is used to solve the interface between air and rubber. VOF is a technique that can track a free surface or an interface between two immiscible fluids. Here a single set of momentum equations is shared by the fluids, and the volume fraction of each fluid is calculated for the entire domain using the VOF transport equation. Its framework does not require a mesh deformation technique to be implemented. An implicit formulation is employed for the temporal discretisation of the VOF transport equation and a highresolution-interface capturing (HRIC) scheme (Tsui et al., 2009) is used for spatial discretization. A time step size of 0.0007 s was employed for all the calculations and a residual criteria of  $10^{-3}$  was used as a convergence criteria.

For performing additional analysis related to distributive mixing behavior in rubber mixing, a set of 2 500 massless particles is also introduced into the domain after an initial period of time. Several statistical quantities are computed through the tracking of these particles. All of these are accomplished via a one-way coupled discrete phase model (DPM). It is called one-way because information passes from the flow field to the particles, but not vice versa. Since the simulations presented here are transient, a total of 15 revolutions of the rotor or 45 s of simulation time are presented.

At the initial time, the rubber and air are assumed to be at rest. With regard to the boundary conditions, a no-slip boundary condition is applied to the chamber and rotor wall boundaries, which means the fluid on the rotor wall will have the same velocity as the rotor itself, and the fluid on the chamber wall will have zero velocity. For the thermal boundary conditions, initially, the temperature of rubber, air, rotor and the chamber wall are all set to be at 313 K. In the large-scale mixer which is typically used in the industry, the mixer is continuously cooled by water or air, and the rate of heat transfer from the polymer melt to the mixer wall can be controlled by changing the flow rate of the coolant fluid. Here, it is assumed that the rotor walls are perfectly cooled and hence, have a constant temperature of 313 K at all times during the simulation. On the other hand, since the polymer melt in the mixer has a very low thermal conductivity, the heat transfer mechanism is dominated by convection. Therefore, a convective heat transfer coefficient of 40 W/m<sup>2</sup> K (Goodyear, 2015) is employed for the chamber wall. The chamber wall is responsible for suppressing the temperature rise of the polymer by extracting heat generated due to viscous heating and dissipating externally to the coolant fluid. While in reality, this coefficient might not be a constant for the entire chamber, it is chosen here as a first approximation towards building a more sophisticated model.

#### 5 Results and Discussion

This section presents results from all the simulations conducted here. A detailed assessment of the different fill factors is carried out in order to understand specifically their effects on dispersive and distributive mixing characteristics. Since the simulations presented are non-isothermal, this section begins with a presentation of the thermal field.

#### 5.1 Thermal Distribution

As mentioned above, the computations are carried out under non-isothermal conditions and so it is appropriate to understand the thermal or temperature distribution and even the heat generation. As the rubber compound considered here is highly viscous, there is expected to be internal viscous heat dissipation due to the internal friction of rubber between the different layers, while undergoing rotating motion. As for the initial condition, temperature of the whole domain is chosen to be 313 K, representing the rubber to be cold before the start of any rotation. For the present study rubber viscosity is estimated by the Carreau-Yasuda model (Vingaard et al., 2007), which is also combined with the temperature dependency (Eq. 8).

Figure 4 shows the evolution of the average temperature throughout the domain for different fill factor cases with time. Firstly, as expected, for all the cases, as time increases, the increase in shear results in increase in velocity, and in turn increase in heat generation and temperature. With regard to the fill factor, the 50% case has the lowest temperature throughout the mixing time, whereas the 90% case has the highest temperature. This is because of the combined effect of velocity and viscosity that leads to this kind of behavior. So an increase in the fill factor results in an increased viscous heat generation and temperature. It is also interesting to note from Fig. 4 that

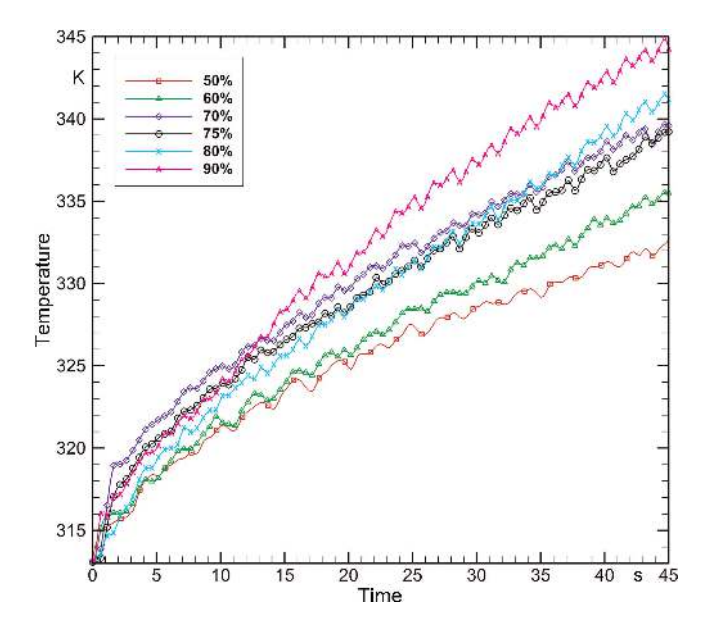


Fig. 4. Evolution of the average temperature distribution throughout the domain with time for the different fill factor cases

the 50% and 60% cases are almost together (at least for most of the simulation) on the lower end of the spectrum, while the 90% case is alone at the higher end of the spectrum. The temperatures for the 70%, 75% and the 80% cases are similar to each other for the entire mixing cycle and are in the middle of the overall temperature range. Figure 5 presents the evolution of the average laminar viscosity of rubber throughout the domain, with time. There is a consistent reduction in viscosity with increase in fill factor and this is due to the increased heat generation resulting from the larger amounts of the rubber in the higher fill factor cases.

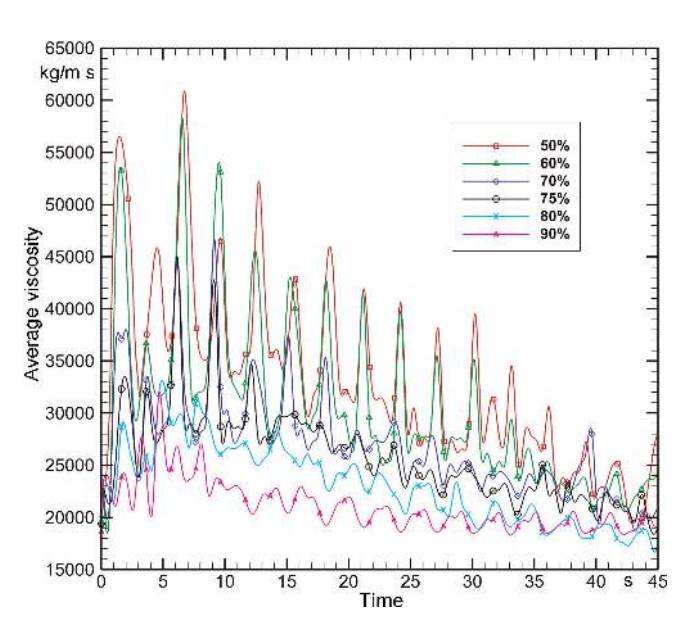


Fig. 5. Average viscosity distribution throughout the domain with respect to time for different fill factor cases

From a previous isothermal study of the same research group (Dhakal, 2016), a 75% fill factor case showed better dispersive and distributive mixing characteristics compared to fill factors such as 45%, 60% and 90%, and hence better goodness of mixing. Hence, it is not surprising that fill factors in and around the 75% range (i.e. 70%, 75% and 80% cases here) show a temperature distribution that is neither too high and neither too low, all of which is an indication of their higher mixing efficiency.

## 5.2 Flow Pattern

Figure 6 shows instantaneous velocity contours of rubber on the plane after 15 revolutions of the rotors. Note that a volume fraction of 1.0 represents pure rubber, and the rubber phase velocities are obtained by only selecting those regions where the volume of fluid >0.5, which is a representation that it is pure rubber in that cell. Cells that have volume of fluid <0.5 are not shown in the figure because their represent pure air based on the criteria used here for post-processing. For all the cases, as expected, the region around the rotor tips experiences higher velocity than the rest of the domain. With increase in fill factor, it can be seen that the area of high velocities keeps increasing, until the 90% fill factor case, which shows very high velocities in the top of the chamber. Also, the 50% and 60% fill factor cases have very low velocities especially behind the rotors tips, in comparison to the other fill factor cases.

#### 5.3 Rubber Volume Fraction

The volume of fluid (VOF) technique is used in this study to track the interface between rubber and air. This technique helps in identifying the computational cells occupied by the rubber during the simulation. Figure 7 represents contours of the rub-

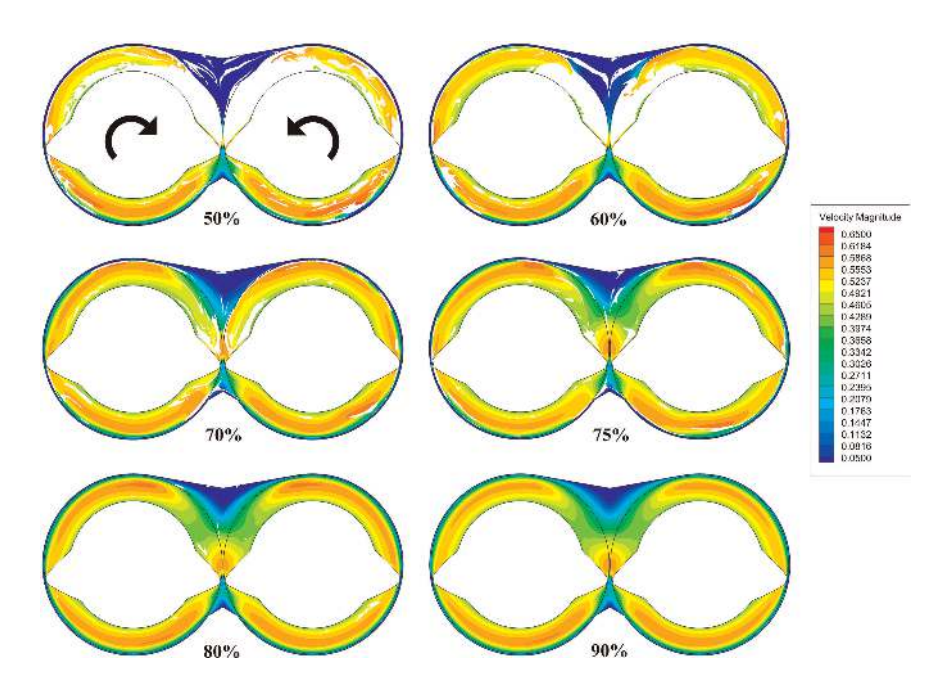


Fig. 6. Instantaneous velocity contours of rubber at t = 45 s, or at 15 rotor revolutions, for the different fill factor cases

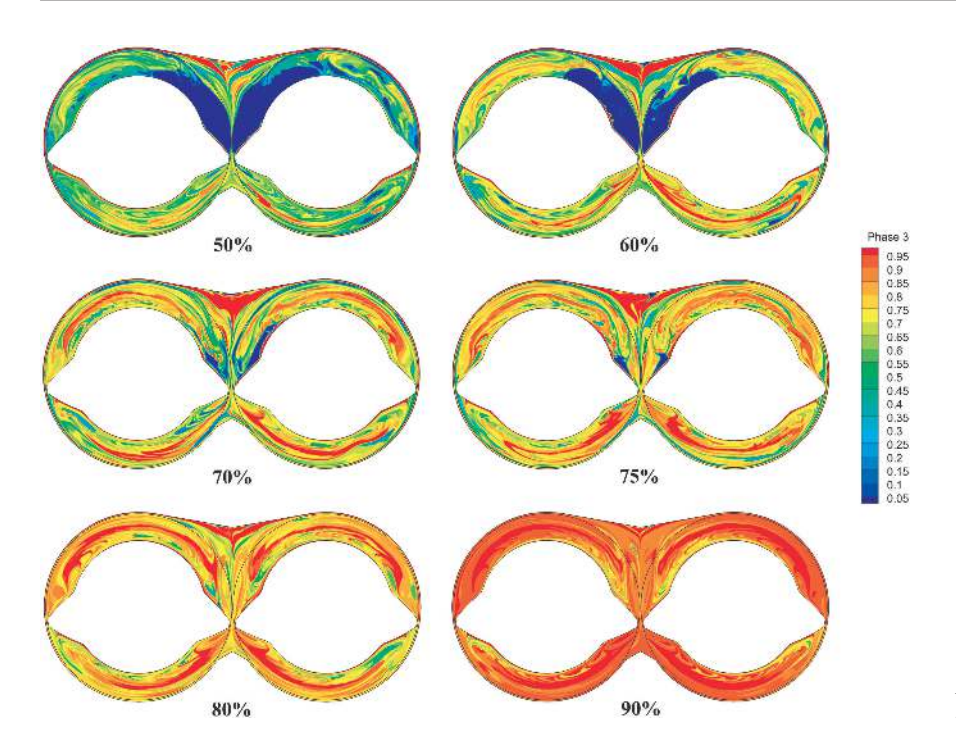


Fig. 7. Volume of Fluid (rubber) after 45 s of running time

ber volume fraction for different fill factor cases after 45 s of simulation time. Again, volume fraction of 1.0 represents pure rubber. These figures are a visual indication of how the rubber is distributed in the entire domain.

The volume fraction can also be used as a crude indicator of the extent of good distributive mixing. For instance, the 50% and 60% fill factor results show a lot of big wide open spaces (or air pockets) between the rotors. This could possibly result in lesser shear in order to break down the agglomerates, or in other words, worse dispersive mixing characteristics compared to other cases. On the other hand, the 90% result shows almost the entire mixing chamber filled with pure rubber, indicating that there are probably not as much open spaces for the rubber to get dispersed and distributed. In this respect, the 70 %, 75 % and 80% cases qualitatively seem to show best distribution of rubber, because visually, there seems to be a good number of air pockets interspersed between the rubber agglomerates. Again, it should be emphasised that such an analysis is purely from a visual point of view, and one cannot quantitatively judge the dispersive and distributive mixing characteristics based on rubber volume fraction distributions. For this purpose, certain specific statistics need to be analyzed, and these are discussed in the detail in the next two sections.

## 5.4 Dispersive Mixing

As mentioned earlier, good dispersive mixing is achieved by shear and elongational forces present in the mixing chamber. The shear stress is the primary reason for breaking the agglomerates and elongational flow characterizes the flow pattern. Studies have previously shown that elongational flow is more effective for agglomerate dispersion in comparison with simple shear flow (Yang and Manas-Zloczower, 1994). For under-

standing and quantifying this flow pattern and its dispersion effects, mixing index and maximum shear stress are presented.

Mixing index is a very common parameter used to quantify dispersive mixing (Collin et al., 2006; Connelly and Kokini, 2004, 2007; Das et al., 2016; Manas-Zloczower, 1997; Vyakaranam and Kokini, 2012). Mixing index can be calculated from the following equation (Manas-Zloczower, 1997):

$$\lambda_{MZ} = \frac{|\dot{\gamma}|}{|\dot{\gamma}| + |\omega|}. \tag{11}$$

Here  $|\dot{\gamma}|$  and  $|\omega|$  represent the shear rate and vorticity tensor, respectively. Mixing index ranges from 0 to 1, with the value of 0 indicating pure rotational flow, 0.5 for simple shear flow and 1 for pure elongational flow. Figure 8 shows the probability density function (PDF) of mixing index calculated over 45 s of mixing time. The PDF represents the number of cells throughout the domain experiencing a value of mixing index within a certain range. Firstly, from the figure, it is clear that the 50% case has the most pure rotational flow compared to all the other cases. The 80% and 90% cases show the best elongation flow characteristics, whereas the 70% case shows the best simple shear flow characteristics. With regard to simple shear flow, although the 70% case is the best, all the other cases except for the 50% case do perform almost as good. So based on the premise that elongational components are the more effective for agglomerate dispersion, the 80% fill factor case seems to be the best for dispersive mixing.

While mixing index is one indicator of effective agglomerate dispersion, it still does not provide any information about regions of high shear that can effectively break the agglomerate (Avalosse et al., 2005). The distribution of maximum shear stress (Manas-Zloczower and Cheng, 1996; Yang and Manas-Zloczower, 1994) is a quantity that can be used to assess dispersive mixing, particularly for a shear-driven flow such as the

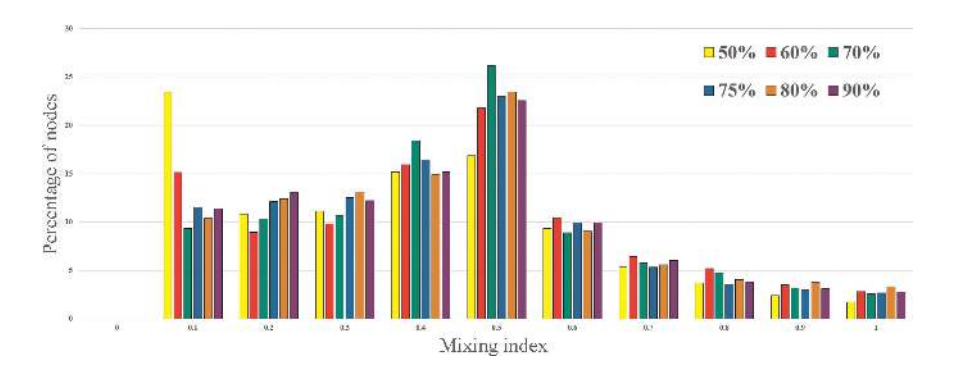


Fig. 8. Probability density function (PDF) of mixing index for the different fill factor cases

problem in the current study with a viscosity of 10<sup>5</sup> Pa s. To achieve this, 2500 massless particles are injected into the domain after 5 revolutions. The shear stress is calculated at the locations of these particles over 10 rotor revolutions and using this data, the cumulative distribution of the maximum shear stress is determined. In addition to mixing index, an important parameter that illustrates the dispersive mixing capability is the maximum shear stress (Manas-Zloczower and Cheng, 1996; Yang and Manas-Zloczower, 1994), particularly for a shear-driven flow such as the problem in the current study with a viscosity of 10<sup>5</sup> Pa s. The higher the shear stress experienced by the ingredient, the greater is the dispersion. Figure 9 shows the cumulative distribution function (CDF) of maximum shear stress calculated over 10 revolutions of the rotors or 45 s of the simulation time. The way to explain the max shear stress behavior is as follows: The CDF of maximum shear stress represents the percentage of particles experiencing a shear stress above a specific value. For instance, if one considers a reference value of the shear stress of 20 kPa, the 70% fill factor case has a CDF value of 70% at this max shear stress, which means that this case will have 30% of particles experiencing a shear stress higher than 20 kPa. The corresponding number for the rest of the fill factors is less, for instance 25 % for the 80 % fill factor case and 10 % for the 90% fill factor case. So the further a curve is towards the right of the plot, the better is its dispersive mixing characteristics. Of course with the assumption of a homogeneous rubber compound for the material employed in these simulations, there is really no information about the shear stress needed for agglomerate breakup. If the critical value required for rupture of filler materials is known, one can determine the number of particles broken down by shear stress (Avalosse et al., 2005). So based on an arbitrarily chosen value of shear stress needed for breakup such as 20 kPa, the 70% fill factor case displays the best dispersive mixing characteristics. These trends hold true for a large part of the range of the maximum shear stress values. So for a threshold between 10 kPa and 30 kPa, 70% fill factor shows the best dispersive mixing. For a threshold shear stress outside this range, the curves are very close to each other with no discernible difference between them.

## 5.5 Distributive Mixing

For good mixing, while the breakup of agglomerates is important, the spatial resolution of the broken agglomerates is also

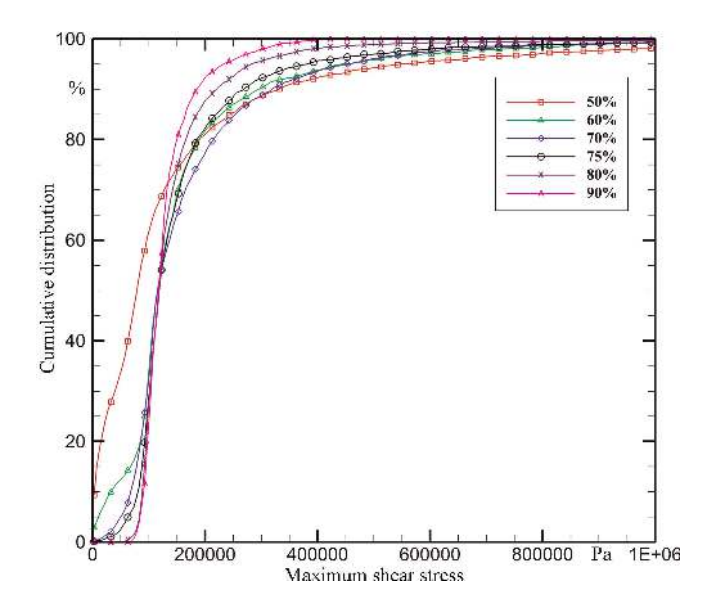


Fig. 9. Cumulative distribution of maximum shear stress for the different fill factor cases

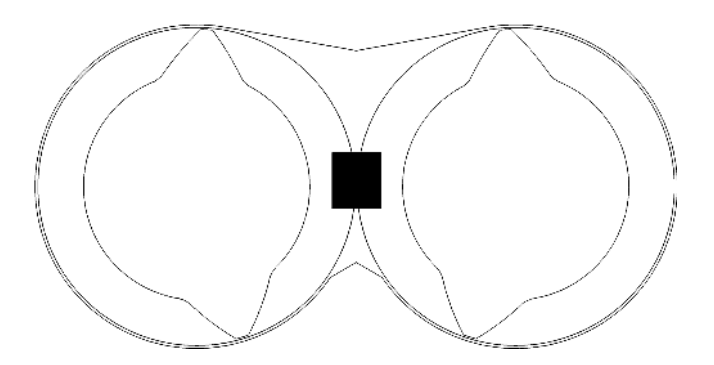


Fig. 10. Initial position of massless particles as form of cluster

critical. This can be quantified by distributive mixing characteristics. As the name suggests, it is a process of distributing the broken particles throughout the domain. In order to calculate all the statistics that can quantify distributive mixing in this paper, tracking of the 2500 massless particles (used for the maximum shear stress calculations above) is carried out. Figure 10 shows the initial position of the set of massless particles inside the domain. As it can be seen in the figure, the particles are in-

jected in the form of a rectangular cluster. Figure 11 shows the instantaneous particle positions after 45 s of mixing time for all the different fill factor cases. Purely by visualization of the particles, it can be inferred from these figures that the particles are clustered together to a larger extent for the 50% and 60% fill factor cases whereas there are slightly more open spaces in the 90% case. The 70%, 75% and 80% cases seem to show the best distribution of particles visually. This distribution of particles can in fact be quantified using parameters such as cluster distribution index (CDI), mean length of stretch (LOS) and scale of segregation (SOS), which are discussed next.

CDI (Connelly and Kokini, 2007) compares the calculated mixing distribution to the ideal one. The ideal distribution is determined by assuming that the particles are uniformly distributed throughout the domain, and hence, it is the most optimum distribution that can be achieved by the mixer. The following equation is used to calculate CDI (Manas-Zloczower, 2012):

$$f(r) = \frac{2}{N(N-1)} \sum_{i} \delta(r'_{i} + r) \delta(r'_{i}) = \int_{r-\Delta r/2}^{r+\Delta r/2} c(r) dr.$$
 (12)

Here, f(r) is the coefficient of the correlation function for the distance between the particle pairs and this represents the probability of finding a neighboring particle in the range of  $r-\Delta r/2$  to  $r+\Delta r/2$  of the  $i^{th}$  particle located at  $r_i'$ . And  $\delta r=1$  represents the fact that the particle is present, otherwise  $\delta r=0$ . c(r) indicates the coefficient of the probability density function of the correlation function, f(r). Note that the area under the curve c(r) is a constant. So

$$\sum_{r=0}^{r=t_{\text{max}}} c(r)\Delta r = 1. \tag{13}$$

Here,  $r_{max}$  is the largest distance of the domain. So no particle can be found at a distance greater than  $r_{max}$ . This means  $c(r > r_{max}) = 0$ . Hence CDI can be defined as:

$$\varepsilon = \frac{\int_0^\infty \left[ c(r) - c(r)_{\text{ideal}} \right]^2 dr}{\int_0^\infty \left[ c(r)_{\text{ideal}} \right]^2 dr}.$$
 (14)

Here, c(r) is the calculated distribution,  $c(r)_{ideal}$  is the ideal distribution and  $\epsilon$  is the CDI, which depends on the initial position and number of the particles. Initially (at t=0), while particles are clustered together  $\epsilon$  should have a large value. After a certain period of time, as the calculated distribution gets closer to the ideal distribution, values of  $\epsilon$  are expected to decrease.

Figure 12 shows the evolution of CDI with time for the different fill factor cases. Here, as expected, initially the values of CDI are higher, and then they decrease with time. The lower the values of CDI, the better is the distributive mixing behavior. The entire range of CDI values are not shown, especially during the initial times (t < 10 s), in order to illustrate the behavior of CDI when the values between the fill factor cases are comparable to each other. The peaks found in the curves are due to stretching and unstretching of the cluster of particles. From the figure it is clear that the 50% case has the worst distributive mixing based on the relatively higher CDI values throughout the mixing cycle. With regard to the best distributive mixing from the point of view of CDI, the 80% and 90% cases are quite close to each other, with the 80% case inching past the 90% for t > 25 s.

Along with CDI, another quantity, called SOS introduced by Danckwerts (1952; 1953), closely describes the mixing behavior. It was used by Tadmor and Gogos (2013) to describe the texture of the mixing and Connelly and Kokini (2007) to quan-

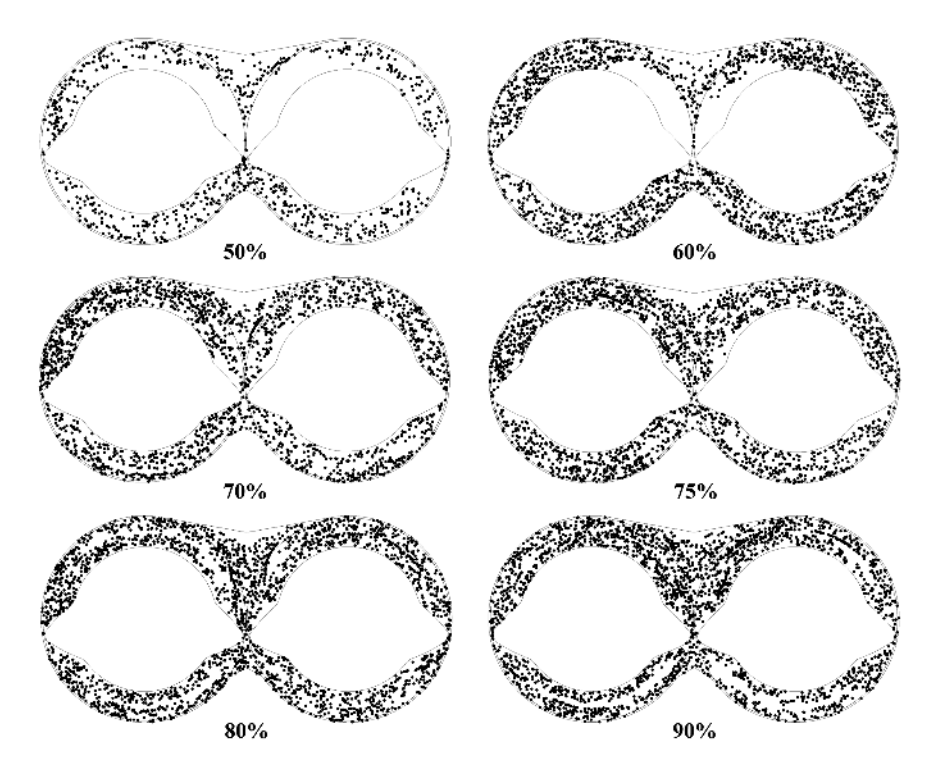


Fig. 11. Distributed particles throughout the domain after completing 15 revolution rotational motion of the rotors for different fill factor cases

tify distributive mixing. SOS is defined by the following equation:

$$L_{s} = \int_{0}^{\zeta} R(r)dr, \tag{15}$$

where

$$R(r) = \frac{\sum_{i=1}^{N} (x_i' - \bar{x})(x_i'' - \bar{x})}{NS^2}.$$
 (16)

Then

$$S^{2} = \frac{\sum_{j=1}^{M} (x_{j} - \bar{x})^{2}}{M}.$$
 (17)

Here, R(r) is the coefficient of correlation which measures the degree of correlation between the concentrations of two particles separated by a distance r. R(0)=1 means that the two particles have the same correlation separated by zero distance. On the other hand,  $R(\zeta)=0$  means that there is no correlation between the particles separated by a distance  $\zeta$ . Again,  $x_i'$  and  $x_i''$  are the concentrations of the  $i^{th}$  pair and  $\bar{x}$  is the average concentration. M is the total number of particles and N is the total number of pairs.  $S^2$  is the variance which is calculated from the concentration of all the particles. j represents the index of the particle, and  $L_s$  is the SOS.

The SOS is calculated as follows: After carrying out the fluid flow and mixing calculation with the particles for a certain period of time (in this case  $t=22\,\mathrm{s}$ , chosen arbitrarily), the particles are tagged according to their current location. So all the particles in the top half of the chamber are assigned a value of zero, whereas the particles in the lower half are assigned a value of 1. The calculations are performed further for another 23 s of simulation time, leading to the now-tagged particles with tags of either zero or 1, being distributed or segregated throughout

the domain. With the whole chamber is divided equally by two portions. Initially a simulation was run for twenty two seconds to give some time for particles to get distributed throughout the region. The time period was chosen arbitrarily. After that, the concentration of the particles that stay in the upper portion were assigned with the value of zero and the particles that stay in the lower portion were assigned with the value of 1. So after running the simulations for a certain period of time, two different types of particles having two different concentrations will be segregated throughout the domain. Therefore with time, the segregation will decrease and by tracking the particles, this can be quantified in the form of SOS. The lower the value of SOS, the better is the distributive mixing.

Figure 13 shows the evolution of SOS with time for the different fill factor cases. As expected, the SOS values are very high initially, because of the two sets of particles with different concentrations (of 0 and 1) separated in the upper and lower portions of the mixing chamber. But with time, they continue to decrease. For instance, at a time of  $t=25\,$  s, the 90% and 70% cases have the lowest and highest SOS values, respectively. Also, the SOS profiles do display some oscillations, an indication of the stretching and unstretching of the material. It is interesting to note that the 80% case has the least oscillations. Overall, it is the 80% case that maintains its low value mainly because of the lower oscillations compared to the rest of the cases. Hence, the SOS shows that the 80% exhibits the best distributive mixing.

Another quantity that is also considered to quantify distributive mixing is LOS, defined by Ottino (1989). LOS is the ratio of the distance between the different particle pairs. This quantity could also be used for determining mixing efficiency (Manas-Zloczower, 1997). The mean LOS can be expressed by following equation:

$$L_{\lambda} = \frac{|X_t|}{|X_0|},\tag{18}$$

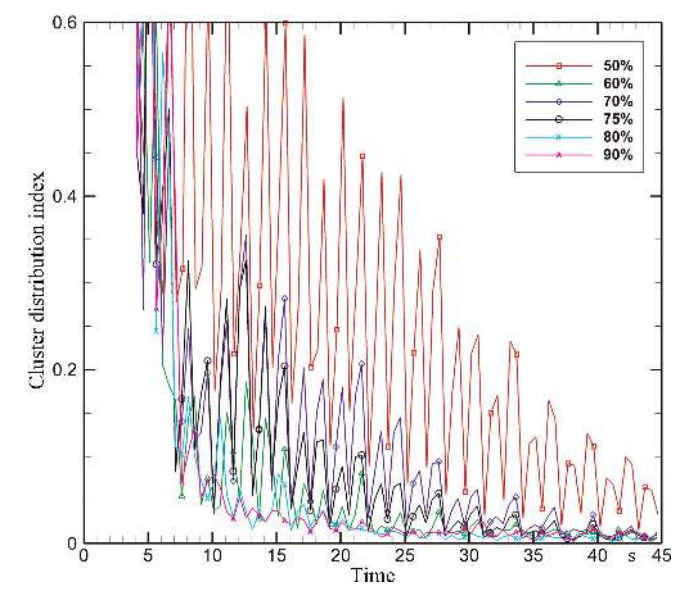


Fig. 12. Evolution of the cluster distribution index (CDI) with time for the different fill factor cases

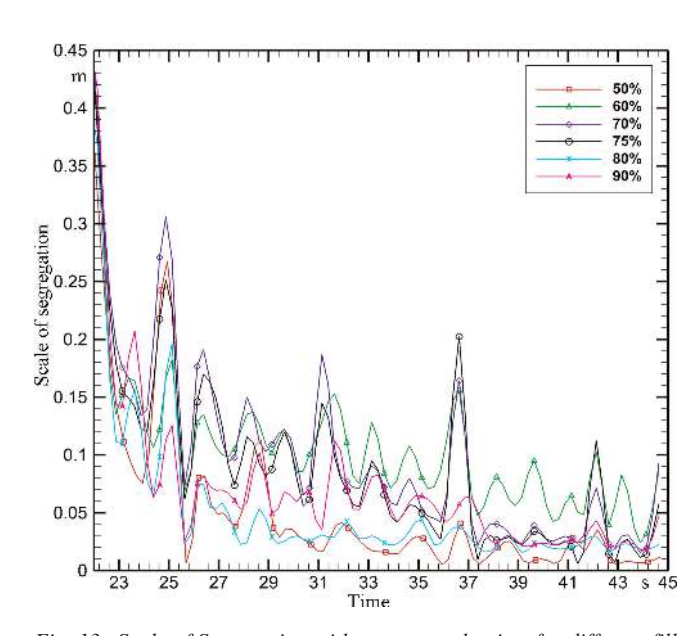


Fig. 13. Scale of Segregation with respect to the time for different fill factor cases

where,  $X_0$  and  $X_t$  are the distances between the particle pairs at the beginning of simulation and at time, t, respectively. For any cluster of particles, it is expected that  $L_{\lambda}$  will increase with time, and the higher the value of LOS, the better is the spatial distribution.

Figure 14A shows the value of evolution of mean LOS with time for the different fill factor cases. As expected, LOS values for all the cases are zero initially and increase with time. The lowest LOS values during the initial period are not shown in the figure in order to focus on the mixing behavior in the later stage of the simulation. It is hard to judge the mixing from the mean LOS plot, mostly because of the oscillations in all the curves. The oscillations are again due to the stretching and unstretching of the material resulting from the rotational motion. The 50% case displays the highest magnitude oscillations, while the 80% case displays the lowest. So, while the 50% case shows high LOS values periodically, indicating better distributive mixing, it also shows low LOS values during other periods, suggesting the opposite trend. To obtain a clearer picture of the LOS behavior, a filtered version of the mean LOS is introduced and presented here. This filtered form is calculated by averaging two consecutive values of the mean LOS. Figure 14B shows the cumulative average of the mean LOS as a function of time. This curve still displays oscillations, but with a much lesser magnitude. Again, in this curve the case 50% shows the highest magnitude oscillations and hence, with its display of the lowest LOS values, one can conclude that the 50 % fill factor case exhibits the worst distributive mixing characteristics. Aside from the 50% case, and on comparing the rest, it can be seen clearly that the 80% fill factor case shows the best distributive mixing with its consistently high LOS values.

#### 6 Conclusions

Two-dimensional non-isothermal numerical simulations of rubber mixing in a chamber partially filled with the material, and equipped with a set of two-wing non-intermeshing counter-rotating rotors are conducted using a commercial CFD code. The model developed here assumes that the material is a highly-viscous Carreau-Yasuda rubber along with a temperature-dependent viscosity. The main objective of the study was

to comprehensively assess the effects of the different fill factors on distributive and dispersive mixing characteristics. Fill factor is the ratio of the volume of rubber to the entire volume of the mixing chamber as a percentage. Six different fill factors of rubber are chosen for this study. They are 50%, 60%, 70%, 75%, 80% and 90%. A fill factor of 50% means that 50% of the volume of the mixing chamber is rubber, while the rest, i.e. 50% is air. Several quantities are presented here to describe qualitatively and quantitatively the mixing behavior.

The presentation of results begins with a description of the thermal distribution. Average temperature throughout the domain was calculated and shown with respect to time. All cases showed a temperature increase due to the internal heat dissipation as a result of the high viscosity of rubber. Understanding the temperature distribution is critical in such applications, because of its impact on choice of material for additives and equipment. Fill factors of 50% and 90% showed the lowest and highest temperatures throughout the mixing cycle, respectively, whereas the 70%, 75% and 80% had similar temperatures, that were in between the extremes. Also, flow pattern in the domain was presented through distributions of velocity magnitude, which showed that 50% and 60% cases had larger regions with lower velocities compared to other cases. Again, relative to these extreme cases the 70%, 75% and 80% cases showed reasonable velocity distributions. In addition, volume fraction helped identify to the open spaces (or air pockets) in the domain. Rubber volume fraction contours were presented to describe visually the impact of the fill factor on the spatial distribution of rubber.

In order to analyze dispersive and distributive mixing in detail, several statistics, mostly Lagrangian, were calculated and presented. The first quantity was called a mixing index calculated to assess dispersive mixing. A probability density function of the mixing index helped to identify the extent of elongation components vs. simple shear components vs. plot flow components. With elongation flow primarily being responsible for agglomerate dispersion, the 80% case displayed the best dispersive mixing characteristics. While mixing index has several advantages in terms of its simplicity and ease of calculation, it still cannot predict the probability of particles going through those high shear regions. For this purpose, a cumulative distribution of the maximum shear stress was presented using a set of massless particles injected into the domain. The

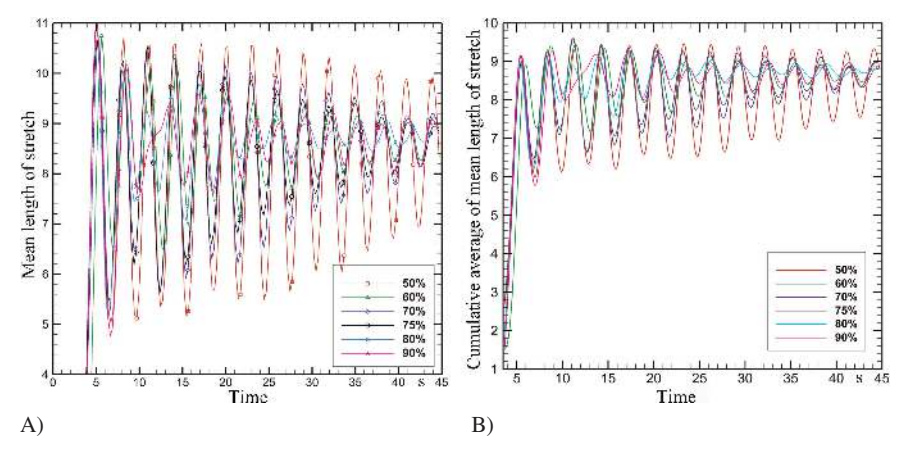


Fig. 14. Temporal evolution of (A) mean length of stretch and (B) cumulative average of mean length of stretch, for the different fill factor cases

physical significance of this quantity is such that if more particles experienced a shear stress higher than a specific value, then the breakup of the agglomerates is easier and more effective. Results of maximum shear stress distribution showed that the 70% fill factor case provided the best results.

Along with breaking up the agglomerates, another factor that determines the goodness of the mixing is the spatial distribution of the broken agglomerates. This is referred to as distributive mixing. Again, several parameters were presented to quantify distributive mixing. CDI or cluster distribution index quantitatively compared the calculated mixing distribution to the ideal distribution. The ideal distribution was calculated by assuming that particles were uniformly distributed throughout the domain. So a lower value of CDI represented a better distributive mixing ability. CDI showed that the 80% fill factor case performed the best. SOS or scale of segregation, another statistic that calculated the separation between tagged particles also showed that 80% had the best distributive mixing abilities. Finally, results of the mean LOS or length of stretch concluded the same as well.

While the simulations presented here are two-dimensional, some valuable insights have been drawn with regard to the effect of fill factor on dispersive and distributive mixing, especially considering the fact that this study presents the first attempt at comprehensively analyzing fill factor in non-isothermal partially-filled rubber mixing simulations. Even though the results do not show a clear winner in terms of mixing efficiency, it can be concluded that in general fill factors between 70% and 80% exhibit the best dispersive and distributive mixing characteristics combined.

## References

- Alsteens, B., Avalosse, T., Legat, V., Marchal, T. and Slachmuylders, E., "Effect of the Full-Slip Condition along Rotors on the Mixing Efficiency of Internal Mixers", SPE ANTEC Tech. Papers, 173– 177 (2003)
- Avalosse, T., Alsteens, B. and Legat, V., "Rotor Shape Design by Numerical Simulation: A New Way to Improve Dispersive and Distributive Mixing in Batch Mixers", Elastomery, 9, 16–24 (2005)
- Avalosse, T., Rubin, Y., "Analysis of Mixing in Corotating Twin Screw Extruders through Numerical Simulation", Int. Polym. Proc., **15**, 117–123 (2000), DOI:10.3139/217.1586
- Avalosse, T., Rubin, Y. and Fondin, L., "Non-Isothermal Modeling of Co-Rotating and Contra-Rotating Twin Screw Extruders", J. Reinf. Plast. Compos., **21**, 419–429 (2002), DOI:10.1177/0731684402021005442
- Bai, Y., Sundararaj, U. and Nandakumar, K., "Nonisothermal Modeling of Heat Transfer inside an Internal Batch Mixer", AIChE J., 57, 2657–2669 (2011), DOI:10.1002/aic.12484
- Cheng, H., Manas-Zloczower, I., "Distributive Mixing in Conveying Elements of a Zsk-53 Co-Rotating Twin Screw Extruder", Polym. Eng. Sci., **38**, 926–935 (1998), DOI:10.1002/pen.10260
- Cheng, J., Manas-Zloczower, I., "Flow Field Characterization in a Banbury Mixer", Int. Polym. Proc., 5, 178–183 (1990), DOI:10.3139/217.900178
- Cheng, J.-J., Manas-Zloczower, I., "Hydrodynamic Analysis of a Banbury Mixer 2-D Flow Simulations for the Entire Mixing Chamber", Polym. Eng. Sci., 29, 1059–1065 (1989), DOI:10.1002/pen.760291102
- Collin, V., Peuvrel-Disdier, E., Alsteens, B., Legat, V., Avalosse, T., Otto, S. and Metwally, M. H., "Numerical and Experimental Study of Dispersive Mixing of Agglomerates", SPE ANTEC Tech. Papers, Pages: 908–912 (2006)

- Connelly, R. K., Kokini, J. L., "The Effect of Shear Thinning and Differential Viscoelasticity on Mixing in a Model 2D Mixer as Determined Using FEM with Particle Tracking", J. Non-Newtonian Fluid Mech., **123**, 1–17 (2004), DOI:10.1016/j.jnnfm.2004.03.006
- Connelly, R. K., Kokini, J. L., "Examination of the Mixing Ability of Single and Twin Screw Mixers Using 2D Finite Element Method Simulation with Particle Tracking", J. Food Eng., 79, 956–969 (2007), DOI:10.1016/j.jfoodeng.2006.03.017
- Cotten, G. R., "Mixing of Carbon Black with Rubber I. Measurement of Dispersion Rate by Changes in Mixing Torque", Rubber Chem. Technol., **57**, 118–133 (1984), DOI:10.5254/1.3535988
- Danckwerts, P., "The Definition and Measurement of some Characteristics of Mixtures", Appl. Sci. Res., Section A, 3, 279–296 (1952), DOI:10.1007/BF03184936
- Danckwerts, P., "Theory of Mixtures and Mixing", Research, 6, 355–361 (1953)
- Das, S. R., Dhakal, P., Poudyal, H. and Chandy, A. J., "Assessment of the Effect of Speed Ratios in Numerical Simulations of Highly Viscous Rubber Mixing in a Partially Filled Chamber", Rubber Chem. Technol., 89, 371–391 (2016), DOI:10.5254/rct.16.83778
- Das, S. R., Poudyal, H. and Chandy, A. J., "Numerical Investigation of Effect of Rotor Phase Angle in Partially-Filled Rubber Mixing", Int. Polym. Proc., 32, 343–354 (2017), DOI:10.3139/217.3346
- Dhakal, P., "Numerical Investigations of the Effect of Fill Factor in an Internal Mixer for Tire Manufacturing Process", unpublished Doctoral Dissertation, University of Akron, Akron (2016)
- Dhakal, P., Das, S. R. and Chandy, A. J., "Investigation of Fill Factor in Two-Wing Rotor Mixing of Rubber by Using Computational Fluid Dynamics", Tire Sci. Technol., 45, 144–160 (2017), DOI:10.2346/tire.17.450204
- Dhakal, P., Das, S. R., Poudyal, H. and Chandy, A. J., "Numerical Simulations of Partially-Filled Rubber Mixing in a 2-Wing Rotor-Equipped Chamber", J. Appl. Polym. Sci., 134, 44250(9) (2017)
- Dhanasekharan, K. M., Kokini, J. L., "Design and Scaling of Wheat Dough Extrusion by Numerical Simulation of Flow and Heat Transfer", J. Food Eng., **60**, 421–430 (2003), DOI:10.1016/S0260-8774(03)00065-7
- Emin, M., Schuchmann, H., "Analysis of the Dispersive Mixing Efficiency in a Twin-Screw Extrusion Processing of Starch Based Matrix", J. Food Eng., **79**, 956–969 (2012)
- Fukutani, K., Higashi, K., Yamada, S. and Yamane, Y., "Numerical Study on Distributive Mixing Characteristics in a Partially Filled Internal Mixer", 184th Technical Meeting of Rubber Division, ACS, Cleveland, Ohio: American Chemical Society, Cleveland, Ohio, USA (2013)
- Goodyear, Private Communication (2015)
- Kim, J. K., White, J. L., "An Experimental and Theoretical Study of Starvation Effects on Flow and Mixing Elastomers in an Internal Mixer", Nihon Reoroji Gakkaishi (Journal of the Society of Rheology, Japan), 17, 203–210 (1989)
- Leblanc, J. L., Lionnet, R., "Determining the Components of Mixing Energy when Preparing Rubber Compounds in Instrumented Internal Mixers", Polym. Eng. Sci., 32, 989–997 (1992), DOI:10.1002/pen.760321503
- Limper, A., Hesse, M., "Investigation of Rotor Blades and the Geometrical Effects on the Flow Behavior in Internal Mixer", in European Rubber Research-Practical Improvements of the Mixing Process, Kelting, K.-U., Kny, M. (Eds.), Institut fuer Kunststofftechnik, Paderborn, Germany, p. 207-218 (2005)
- Liu, J., Li, F., Zhang, L. and Yang, H., "Numerical Simulation of Flow of Rubber Compounds in Partially Filled Internal Mixer", J. Appl. Polym. Sci., 132, 42496(8) (2015)
- Malkin, A. Y., Baranov, A. and Balinov, A., "Modeling Non-Isothermal Mixing in a Rotor Mixer", Int. Polym. Proc., **14**, 115–121 (1999), DOI:10.3139/217.1530
- Manas-Zloczower, I., "Analysis of Mixing in Polymer Processing Equipment", Rheol. Bull., **66**, 5–8 (1997)
- Manas-Zloczower, I.: Mixing and Compounding of Polymers: Theory and Practice. Hanser Publishers, Munich (2012)

- Manas-Zloczower, I., Cheng, H., "Analysis of Mixing Efficiency in Polymer Processing Equipment", Macromol. Symp., 112, 77–84 (1996), DOI:10.1002/masy.19961120112
- Manas-Zloczower, I., Nir, A. and Tadmor, Z., "Dispersive Mixing in Rubber and Plastics", Rubber Chem. Technol., 57, 583-620 (1984), DOI:10.5254/1.3536021
- Nassehi, V., Ghoreishy, M., "Modeling of Mixing in Internal Mixers with Long Blade Tips", Adv. Polym. Technol., **20**, 132–145 (2001), DOI:10.1002/adv.1011
- Nikiel, L., Mason, R. and Wampler, W., "Advances in Filler Dispersion Measurements", Rubber Chem. Technol., 89, 142–153 (2016), DOI:10.5254/rct.15.85923
- Osswald, T., Hernández-Ortiz, J.: Polymer Processing: Modeling and Simulation, Hanser Publishers, Munich (2006), DOI:10.3139/9783446412866
- Ottino, J. M.: The Kinematics of Mixing: Stretching, Chaos, and Transport, Volume 3, Cambridge University Press, Cambridge, UK (1989)
- Poudyal, H., Dhakal, P., Das, S. R. and Chandy, A.: Numerical Simulations of the Effects of Rotor Speed in Non-Isothermal Partially-Filled Rubber Mixing, Rubber Division, American Chemical Society, Pittsburg, PA, USA (2016)
- Rathod, M. L., Kokini, J. L., "Effect of Mixer Geometry and Operating Conditions on Mixing Efficiency of a Non-Newtonian Fluid in a Twin Screw Mixer", J. Food Eng., 118, 256–265 (2013), DOI:10.1016/j.jfoodeng.2013.04.020
- Salahudeen, S. A., Elleithy, R. H., Alothman, O. and Alzahrani, S., "Comparative Study of Internal Batch Mixer Such as Cam, Banbury and Roller: Numerical Simulation and Experimental Verification", Chem. Eng. Sci., 66, 2502–2511 (2011), DOI:10.1016/j.ces.2011.02.017
- Tadmor, Z., Gogos, C. G.: Principles of Polymer Processing. John Wiley & Sons., Hoboken, NJ, USA (2013)
- Takeshi, I., Shin-Ichi, K. and Kazumori, F., "3D Non-Isothermal Flow Field Analysis and Mixing Performance Evaluation of Kneading Blocks in a Co-Rotating Twin Screw Extruder", Polym. Eng. Sci., 41, 840–849 (2001), DOI:10.1002/pen.10781
- Takeshi, I., Shin-Ichi, K., Kazumori, F., Teruo, A. and Kazunori, Y., "Numerical Simulation and Experimental Verification of Nonisothermal Flow in Counter-Rotating Nonintermeshing Continuous Mixers", Polym. Eng. Sci., 40, 365–375 (2000), DOI:10.1002/pen.11170

- Takeshi, I., Tarou, A., Shin-Ichi, K. and Kazumori, F., "Flow Patterns and Mixing Mechanisms in the Screw Mixing Element of a Co-Rotating Twin Screw Extruder," Polym. Eng. Sci., 42, 925–939 (2002), DOI:10.1002/pen.11002
- Tsui, Y.-Y., Lin, S.-W., Cheng, T.-T. and Wu, T.-C., "Flux-Blending Schemes for Interface Capture in Two-Fluid Flows", Int. J. Heat Mass Transf., **52**, 5547–5556 (2009),
  - DOI:10.1016/j.ijheatmasstransfer.2009.06.026
- Vingaard, M., Endelt, B. Ø. and Christiansen, J. D. C., "Implementation of a Material Model with Shear Rate and Temperature Dependent Viscosity", European Is-dyna Users' Conference, Gothenburg, Sweden (2007)
- Vyakaranam, K. V., Kokini, J. L., "Prediction of Air Bubble Dispersion in a Viscous Fluid in a Twin Screw Continuous Mixer Using FEM Simulations of Dispersive Mixing", Chem. Eng. Sci., 84, 303–314 (2012), DOI:10.1016/j.ces.2012.07.014
- Wang, W., Manas-Zloczower, I., "Temporal Distributions: The Basis for the Development of Mixing Indexes for Scale-Up of Polymer Processing Equipment", Polym. Eng. Sci., 41, 1068–1077 (2001), DOI:10.1002/pen.10807
- Wu, S., "Calculation of Interfacial Tension in Polymer Systems", J. Polym. Sci. Polym. Symp., 34, 19–30) (1971)
- Yang, H.-H., Manas-Zloczower, I., "Analysis of Mixing Performance in a Vic Mixer", Int. Polym. Proc., 9, 291–302 (1994), DOI:10.3139/217.940291

Date received: April 02, 2018 Date accepted: June 19, 2018

Bibliography DOI 10.3139/217.3694 Intern. Polymer Processing XXXIV (2019) 2; page 182–194 © Carl Hanser Verlag GmbH & Co. KG ISSN 0930-777X